JOURNAL OF CATALYSIS 120, 182–191 (1989)

The Catalytic Effect of Boron Substitution in ZSM–5 Type Zeolites

U. CORNARO* AND B. W. WOJCIECHOWSKI†

*Snamprogetti, Milan, Italy; and †Chemical Engineering Department, Queen's University, Kingston, Ontario, Canada K7L 3N6

Received November 1, 1988; revised April 12, 1989

A homologous series of boron-containing MFI-type zeolites has been prepared and studied for catalytic activity. We find that boron is incorporated into the catalyst lattice and exhibits catalytic activity for one of the least demanding hydrogen conversions, double bond shift. It shows no activity for the next more demanding process, skeletal isomerization. We also find that boron enhances the formation of surface oligomers but lacks the acidity to crack these species. The result is that the presence of boron in an aluminum-containing MFI catalyst causes enhanced coke formation and an increased rate of catalyst decay. These results are confirmed by runs done on a silicalite synthesized from the same starting materials as those of the other catalysts. This sample showed no detectable catalytic activity.

INTRODUCTION

The structure of zeolites of MFI type includes ZSM–5, which is the trade name of one of the variants. Aluminum-containing MFI-type zeolites exhibit catalytic activity and shape selectivity in acid-catalyzed reactions. The incorporation of boron in such structures has been claimed since 1978 (*1*). Definitive evidence of boron occupying a framework position has been provided using various techniques (*2–4*). However, the nature of the boron site is still under debate as to both its structure and its acidity (*5, 6*).

Based on various chemico-physical characterizations (HNMR, IR, NH_3-TPD) (*4, 7, 8*) and reaction tests (*5*), it has been proposed that catalytic activity of the boron site is very low and easily masked by minute impurities of aluminum. For this reason an attempt to characterize the catalytic effects of boron sites must carefully account for the activity of any residual aluminum sites.

In this work, we have prepared a series of catalysts having the same amount of aluminum per unit cell and varying amounts of boron. Pure Al–MFI and B–MFI zeolites and silicate were synthesized for reference. Various morphological, chemical, and physical properties were evaluated for this series of materials in order to isolate the catalytic effect of boron. 1-Hexene double bond isomerization was chosen as a test reaction because the acid strength required for this reaction is low.

EXPERIMENTAL

Zeolite Synthesis and Pretreatments

Zeolites were prepared according to the Snamprogetti procedure (*9*). High purity reagents were used in order to minimize aluminum content. Tetraethoxysilane (Dinasil-A supplied by Dynamit Nobel) was used as a silica source. Aluminum isopropylate and boric acid were supplied by Carlo Erba. Tetrapropylammonium hydroxide (20 wt%, aqueous solution, supplied by Berg Chemie) was used as a templating agent. Reaction mixtures were prepared by hydrolysis of the alkoxy compounds in an aqueous solution containing the templating agent and boric acid. Reaction mixtures whose compositions are reported in Table 1 were aged overnight. Crystallization was carried out in stirred 5-liter autoclaves at 150°C for 3 days. Sample 3, the Al–MFI zeolite, was crystallized for 7 days. Raw zeolites (P) were characterized by TGA and IR. Calcined forms (C) were obtained by thermal decomposition of the organic base

0021-9517/89 $3.00

TABLE 1

Zeolite Synthesis: Gel Composition

Sample	Si/Al	Si/B	TPA/Si	H_2O/Si
1	100	1.25	0.4	40
2	100	5.00	0.4	40
3	100	—	0.4	40
4	—	1.25	0.4	40

at 550°C for 5 h in air. These were then characterized by IR and analyzed for B and Al content. Catalysts 1 to 4 were obtained by ion exchange with an NH_4^+ solution (ca. 1 *M*) followed by the thermal decomposition of the ammonium ion. The catalysts were then characterized by XRD, IR, and SEM and analyzed for Si, B, and Al content.

Zeolite Characterization

Chemical compositions of our zeolites in the H^+ form were obtained by chemical analysis. Silicon was determined gravimetrically; aluminum and boron were determined using inductive coupled plasma analysis. Aluminum content in sample 4, the boron–MFI catalyst, was carefully checked by atomic adsorption using suitably diluted standards. Less than 5 ppm of aluminum was detected. The organic cation present in raw zeolites was determined by weight loss. These experiments were done on a TGA apparatus (Mettler, TA300) in flowing N_2 at a heating rate of 3°C/min.

The crystallinity of zeolites was determined by X-ray diffraction (Philips diffractometer, Cu$K\alpha$ radiation) and FTIR (Nicolet 20 SXC, KBr pellets). Unit cell parameters were obtained using published methods (*2*). The morphology of the crystals was determined using SEM (Philips PSEM 5000).

A pure silicalite was synthesized from the same materials as those used to prepare the other catalysts. XRD and IR studies showed the resulting material to have a pure MFI structure. The morphology of the particles of this product was very similar to that of the active catalysts.

Reaction Test

Isomerization of 1-hexene at 200°C was studied on catalysts 4(B), 3(Al), and 1(B–Al) and the silicalite using an integral, fixed bed, plug flow reactor. The apparatus and procedure were similar to those described in previous studies (*10*). Feed composition is given in Table 2. For each catalyst a series of runs at different times on stream, for various catalyst/1-hexene ratios (cat/oil ratios), was carried out. Liquid and gaseous products, integrally collected, were analyzed using Varian 3700 and Carle SX114S gas chromatographs, respectively. Regeneration and coke analysis were carried out using air at 400°C to burn off the residue, then trapping and weighing the resultant H_2O and CO_2 on dryerite and ascarite columns.

In this way, integral reactant conversion ($\bar{X}_r$) as a function of run duration (t_f) was obtained. From this, using the time on stream theory of catalyst decay (*11*) and a published kinetic model (*12*), the reaction parameters were evaluated. For each reaction product, the time-averaged yield sampled from $t = 0$ to $t = t_f$ was plotted against $\bar{X}_r$. Each of these plots can be enveloped by a single curve, the optimum performance envelope (OPE), which describes the selectivity behavior of a product as t_f approaches 0. The shape of these curves enables us to distinguish between primary and secondary, stable and unstable products.

TABLE 2

Reaction Test: Feed Composition Wt%

Component	Wt%
1-Hexene	97.33
2-Hexene-*cis*	.16
2-Hexene-*trans*	.36
2-Ethyl-1-butene (+hexane)	2.10
3-Hexene	.05

RESULTS AND DISCUSSION

Synthesis and Characterization

The results of chemical analysis of samples 1 to 4 are summarized in Table 3. The total amount of TPA per unit cell was evaluated from weight loss measured with TGA. Decomposition of organic base begins at 400°C. The observed value of ca. 4 TPA/uc is in agreement with previous observations (*13*) and corresponds to 1 TPA molecule per channel intersection. Zeolites 1 and 2 were synthesized in the presence of the same amount of aluminum and different amounts of boron and contain the same amount of aluminum and different amounts of boron, as expected.

Crystallinity of the samples was measured with XRD. The ratio of absorbance of 560/450 cm^{-1} bands is known to depend on the degree of crystallization (*14*) and for our samples lies in the 0.54–0.59 range, in agreement with published values for good crystals.

The morphology of our crystals was observed using SEM. In all cases, agglomerates of microcrystals were observed (Table 4). Microcrystal dimensions are of the same order of magnitude in all samples. We do not expect any influence of this parameter on catalytic behavior.

Boron incorporation in the framework was studied by XRD measurement of unit cell volume on the H^+ form of zeolites. Substitution of Si by B results in unit cell contraction. Integrated absorption ratios for 920/550 cm^{-1} bands were also related to boron content. See Fig. 1.

The Nature of the Boron Site

The symmetry and coordination of a boron site strongly depend on its hydration state. It has been shown by Coudurier and Auroux (*15*) that samples of H–BAlZSM5 exposed to atmospheric moisture show the presence of two different boron sites as observed via 11B-NMR. Site 1 is predominant and was attributed to a tetrahedral BO_4. Site 2 was tentatively attributed to highly distorted tetrahedral framework boron defects such as $(HO)_x$, (H_2O)–B–$(OSi)_y$ ($x + y = 4$; $x = 1, 2$). A new site appears when an H–BZSM–5 is completely dehydrated (site 3) and was attributed to a trigonal BO_3 (*16*).

The nature of the boron site can also be studied using MID-IR spectroscopy. MFI zeolites exhibit IR bands near 1230, 1100, 800, 550, and 450 cm^{-1}. Attributions of these bands were proposed by various authors (*17, 18*). IR spectra of our zeolite 4 (B-MFI) as first made (4P), after thermal treatment (4C), after ion exchange, and after a second thermal treatment (4H) are reported in Fig. 2a. The bands observed in the 900–930 and 1350–1450 cm^{-1} regions are common to all B-containing zeolites and do not appear in zeolite 3, the one containing aluminum, as seen in Fig. 2b.

In Fig. 2a the sample 4P exhibits bands at 1470, 1460, and 1380 cm^{-1} due to CH_3 and

TABLE 3

Chemical Analysis and Unit Cell Volume[a]

Sample	B_2O_3 (wt%)	Al_2O_3 (wt%)	Si/B_2	Si/Al_2	B/uc	Al/uc	TPA/uc	V (Å^3)
1	1.29	0.71	82.5	219.4	2.25	0.85	4.1	5289.8
2	0.86	0.80	128.0	201.5	1.45	0.92	4.1	5310.8
3	0	0.78	—	211.0	0	0.90	4.5	5351.7
4	2.11	[b]	51.5	—	3.58	0	3.9	5257.4

Note. The TPA/uc was determined on precursors of the catalysts.

[a] Orthohombic unit cell for samples 1, 2, 4. Monoclinic unit cell ($\alpha = 90.2$) for sample 4.

[b] Less than 5 μg Al/g zeolite.

TABLE 4

Morphology of Crystals: Dimension in μm

Sample	Agglomerates	Microcrystals
1	0.5–1.5	<0.05
2	20–50	0.1–0.2
3	20–50	0.1–0.2
4	0.5–2	<0.05

CH_2 group deformation of the tetrapropylammonium ion present in the zeolite channels. An adsorption band at 907 cm^{-1} is related to vibrations of boron-containing bonds and is present in all boron-containing zeolites but absent in the one containing aluminum.

Thermal treatment (sample 4C) leads to the appearance of a broad band around 1400 cm^{-1} with a shoulder at 1380 cm^{-1} and shifts the 907-cm^{-1} band to 920 cm^{-1}, while the spectral features attributed to TPA disappear. Thermogravimetric analysis has also shown that after this treatment, the TPA ion has been completely burned out.

Bands at 920 and 1380 cm^{-1} are also observed in borosilicate glasses (*19*) and were attributed to B–O stretching vibrations with silicons as the nearest neighbors of the boron atom. It is known that removal of degeneracy for BO_4 stretching (tetrahedral symmetry around boron) in a calcium borosilicate (*26*) leads to the appearance of bands at 1130 and 926 cm^{-1}. Although literature data do not allow us to assign the 920-cm^{-1} band to tetrahedral or trigonal boron unambiguously, the correlation observed between the 920/550 integrated absorption ratio and unit cell volume contraction strongly suggests to us that this band should be attributed to a boron site linked via oxygen bridges to silicon atoms. Cell parameters are also affected in a way which agrees with this assignment, as seen in Fig. 3.

The origin of the 1400-cm^{-1} band relates to the fact that boric acid exhibits a broad-band around 1430 cm^{-1} attributed to a fundamental vibration plus overtones of out-of-plane vibrations involving (B–OH · · · OH–B) groups (*21*). Taft (*20*) observed that hydration of borosilicate glasses leads to the appearance of a band at 1450 cm^{-1} as a shoulder of the nearby B–O–Si absorption peak. This suggests a tentative attribution of the 1400-cm^{-1} band observed on H^+ and calcined forms of boron-containing MFI to extraframework boric acid or to defective species $(HO)_x$, (H_2O)–B–$(OSi)_y$ proposed by Coudurier and Auroux (*15*). Formation of these species during thermal treatment has to be related to a thermal instability of boron within the lattice, as evidenced by ion exchange, in which part of the boron is leached out (Table 5). We do not observe any shift of 1400, 1380, and 920 cm^{-1} bands in the IR spectra of the H^+ form of boron-

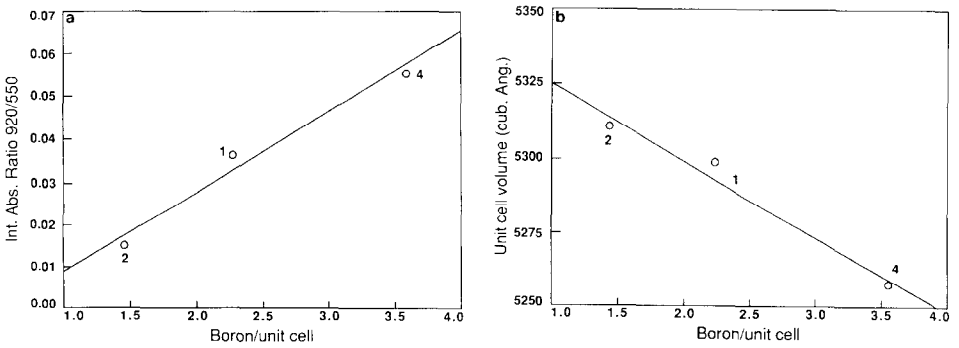

FIG. 1. (a) Integrated absorbance ratio of the 920/550 cm^{-1} bands and (b) unit cell volume for catalysts 1, 2 = B–Al–MFI; 4 = B–MFI.

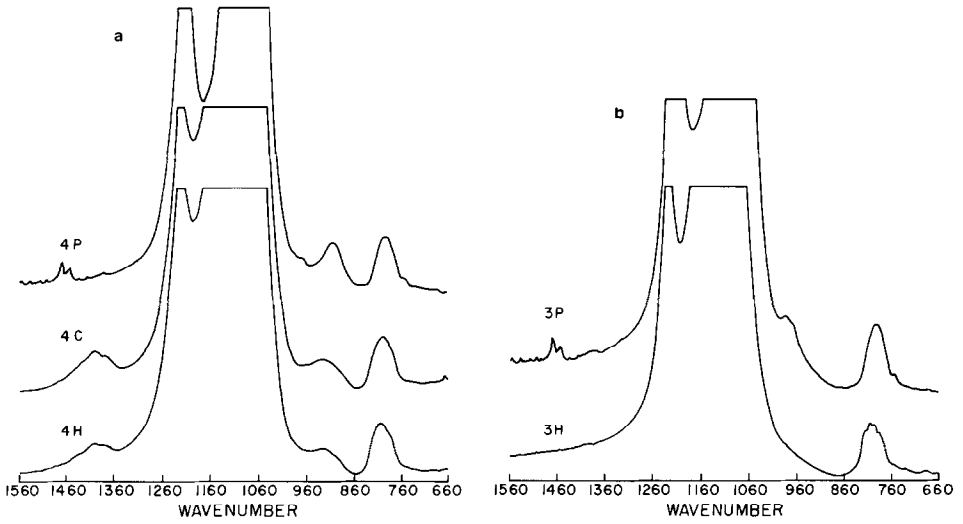

FIG. 2. (a) Infrared spectra. (a) Catalyst 4 = B–MFI: as made (4P); after thermal treatment (4C); in H^+ form (4H); (b) catalyst 3 = Al–MFI: as made (3P); in H^+ form (3H).

containing samples, only a decrease in their prominence.

A quantitative determination of extra-framework and framework boron species would require a combination of 11BNMR, chemical analysis, and XRD studies. However, based on our IR and XRD data and according to cited literature we can say that:

(a) The boron site has an intrinsic low thermal stability.

(b) Boron-containing zeolites in their H^+ form must contain some framework boron, as demonstrated by the correlation of the integrated absorbance ratio for 920/550 cm^{-1} bands and unit cell volume contraction.

(c) Defective boron species formed during the calcination step and responsible for the 1400-cm^{-1} band are also present.

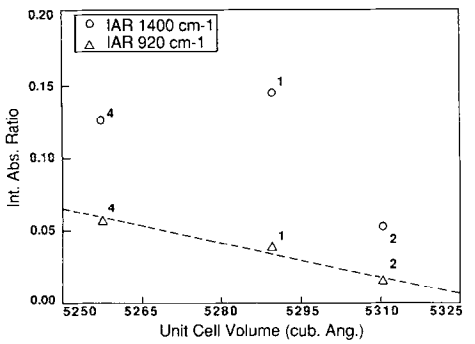

FIG. 3. Boron IR bands: unit cell volume for catalysts 1, 2 = B–Al–MFI; 4 = B–MFI.

Reaction Test

Isomerization of 1-hexene was studied on catalysts 3, 1, and 4 at 200°C. No thermal conversion was observed. In Figs. 4a–c integral conversion of 1-hexene versus time on stream is plotted for the catalysts studied. All catalysts, including 4, showed catalytic activity. Catalyst 1 exhibits activity higher than that of catalyst 3 (Fig. 4d). We conclude, therefore, that boron has activity for the conversion of 1-hexene at 200°C.

The silicalite sample, "exchanged" into the H^+ form, was tested under the same conditions as those of the other catalysts and showed no activity. In order to confirm

TABLE 5

Boron Leaching in the Ion Exchange Step

Sample	1C	1	2C	2	4C	4
Si/B_2	56.2	82.5	125.2	128.0	25.7	51.5

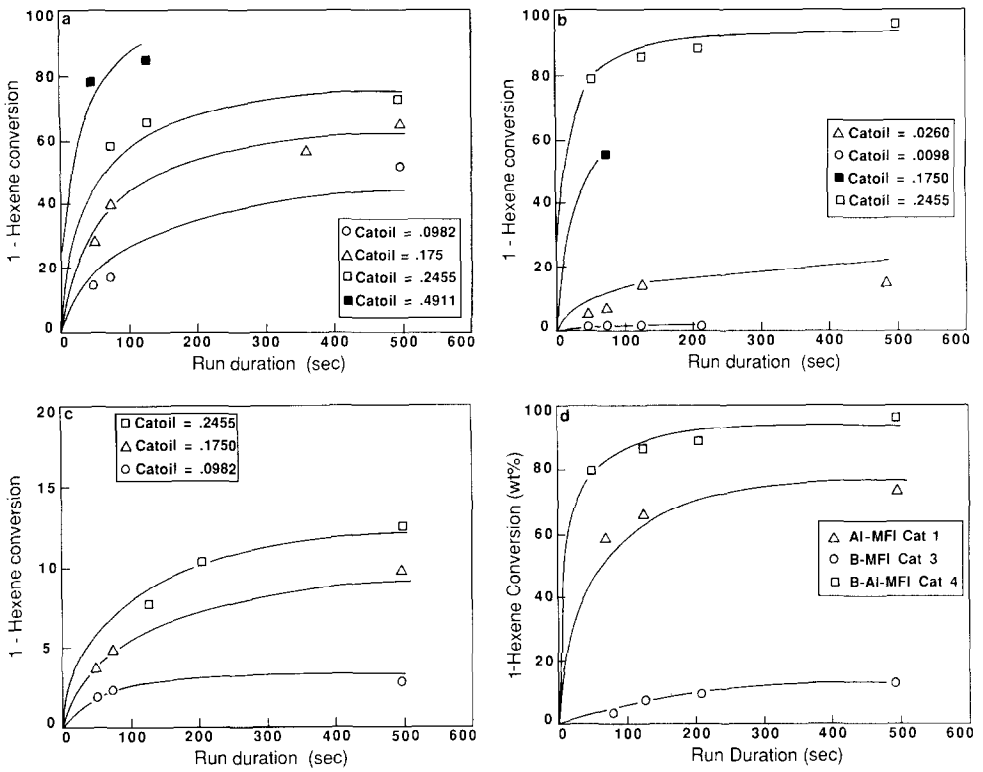

FIG. 4. Conversion plots: (a) catalyst 3 = Al–MFI; (b) catalyst 1 = B–Al–MFI; (c) catalyst 4 = B–MFI. (d) Comparison of conversion at constant cat/oil ratio for catalysts 1 = B–Al–MFI; 3 = Al–MFI; 4 = B–MFI.

this result, we performed a series of runs at cat/oil ratios up to 2.25, some 10 times higher than those shown in Fig. 4, and found less than 1%, i.e., zero within our limits of error, conversion at even this extreme condition.

Results obtained for catalysts 3 and 1 were fitted by a first-order kinetic expression derived from the time on stream theory of catalyst decay (*11*) and a Langmuir based kinetic model (*12*):

$$\frac{dX_r}{d\tau} = \frac{(1 + Gt)^{-N} * A(1 - X_r)}{1 + B(1 - X_r)}.$$

Parameters A, B, G, N were optimized to obtain the best fit to the experimental data. Optimized G and N parameters are related to m and k, the order and the kinetic constant for catalyst decay. It is clear that catalyst 1 decays faster, the decay order being the same (Table 6) for both catalysts. This indicates that although the mechanism of decay in both catalysts is the same, the presence of boron in the catalyst speeds up the deactivation reaction. Table 8 shows that boron also encourages coke formation.

Selected yields versus conversion plots are presented in Figs. 5a–d. Each product can be classified as primary or secondary, stable or unstable. Initial selectivities for all primary products were, therefore, evalu-

TABLE 6

Optimum Values for G, N Parameters: Kinetic Model Based on Time on Stream Theory of Catalyst Decay

Sample	G	N	m	k (min^{-1})
1	3.44	1.00	2.00	3.44
3	2.05	0.98	2.02	2.01

Note. 1-Hexene isomerization reaction at 200°C.

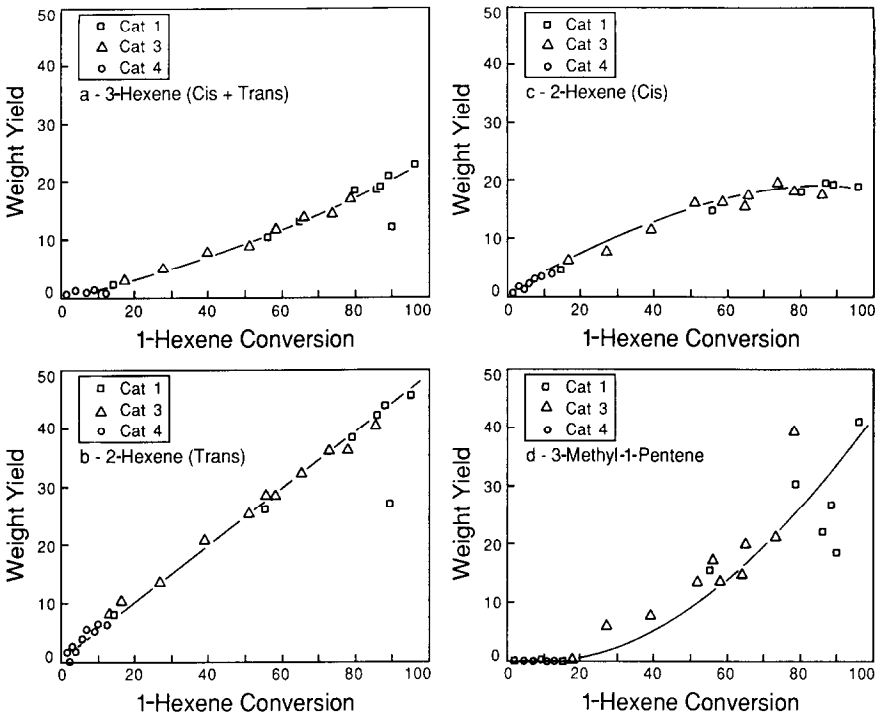

FIG. 5. Selectivity for total 3-hexene *cis* + *trans*; (b) selectivity for *trans* 2-hexene; (c) selectivity for *cis* 2-hexene; (d) selectivity for 4-methyl-1-pentene.

ated from slopes of the OPEs at the origin.

As observed previously (*22*), 2-ethyl-1-butene, present as a major impurity in the feed, rapidly decreases in concentration and its disappearance is directly related to the formation of 3-methyl-2-pentene. Our results are summarized in Tables 7 and 8 and fall in line with previous work (*23*). To begin with, on all three catalysts, double bond shift is the dominant reaction. We believe that interaction of the olefin with an acid site leads to the formation of a carbenium ion (I) (Fig. 6). Deprotonation, hydrogen transfer, cyclization, or oligomerization can now occur. 3-Hexene isomers are obtained via a hydrogen shift rearrangement of carbenium ion (I). 2-Hexene isomers are obtained via deprotonation from carbenium ion (I) or from carbenium ion (II). The initial selectivities for 3-hexene isomers are considerably lower than the initial selectivities for 2-hexene isomers, suggesting that the rate of deprotonation is greater than the rate of hydrogen transfer necessary to form 3-hexene.

The *cis*/*trans* 2-hexene isomer ratio of 0.61 and *cis*/*trans* 3-methyl-2-pentene isomer ratio of 1.8 are greater than the expected thermodynamic equilibrium values (respectively 0.39 and 0.66 (*24, 25*)). The excess of the *cis* isomer suggests that steric effects on the parent carbenium ion (I) lead

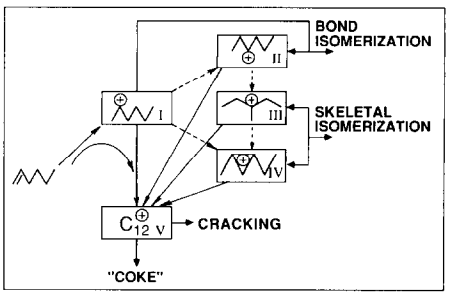

FIG. 6. Suggested intermediates in the isomerization of 1-hexene.

TABLE 7

1-Hexene Isomerization Reaction at 200°C

Reaction product	Catalyst		
	3	4	1
Double bond isomerization			
2-Hexene *cis*	1u	1u	1u
2-Hexene *trans*	1s	1s	1s
3-Hexene (*cis* + *trans*)	(1 + 2)s	1u	(1 + 2)s
Skeletal isomerization			
3-Methyl-2-pentene *cis*	2s		2s
3-Methyl-2-pentene *trans*	2s		2s
4-Methyl-2-pentene *cis*	2s		2s
4-Methyl-2-pentene *trans*	2s		2s
2-Methyl-pentene	2s		2s
4-Methyl-1-pentene	2s		2s
3-Methyl-1-pentene	2s		2s
Oligomerization-cracking			
Alkenes C12	2s		2s
Alkenes C10	2s		2s
Alkenes C9	2s		2s
Alkenes C8			
Alkenes C7	2s		2s
1-Pentene	2s		2s
2-Pentene *cis* + *trans*	2s		2s
2-Methyl-1-butene	2s		2s
2-Methyl-2-butene	2s		2s
Isobutene	2s		2s
2-butene *cis*	2s		2s
2-butene *trans*	2s		2s
Propylene	2s		2s
Ethylene	2s		2s
Hydrogen transfer			
3-Methylpentane	2s		2s
Pentane	2s		2s
2-Methyl-1-butane	2s		2s
Isobutane	2s		2s
Butane	2s		2s
Coke formation			
Coke	1s	1s	1s

to a preferential formation of the *cis* isomers. This effect has been reported previously (*23*).

Coke is a primary product on all the catalysts. From the decay constants and from initial coke selectivities, we note that boron-containing catalysts foul and decay faster. No aromatic products or products with more than 12 carbon atoms were detected in the product. This also agrees with previous reports on H–ZSM–5. The hydrogen/carbon ratio in coke is ca. 2 and suggests the presence of undesorbed oligomers, as was also shown using FTIR studies (*27*).

Skeletal isomerization products are found as secondary products on catalysts 3 and 1, those containing aluminum. No traces of skeletal isomerization are observed on catalyst 4, which contains only boron. This constitutes an indication that boron presents weaker acid sites for catalysis. Differences between the catalysts are also evident when total skeletal isomerization yield is plotted versus log (τ/b), where τ, the space time, is defined as

$$\tau = b * \text{Catoil} * t_f$$

and b is the ratio of the density of gaseous feed divided by the density of the catalyst (Fig. 7).

Skeletal isomerization products are formed via deprotonation of a branched carbenium ion such as (III). Carbenium ion (III) in turn is formed by a sequence of H shifts and methyl shifts and/or via a cyclopropyl carbenium ion intermediate (IV). It seems that boron sites are not capable of either of these energetically demanding steps. The very low acid strength of boron acid sites is thus confirmed by their kinetic behavior.

The higher activity observed for catalyst 1 compared with catalyst 3 can be attributed to the presence of boron and alumi-

TABLE 8

Hexene Isomerization Reaction at 200°C: Weight Selectivity for Primary Products

Reaction	Product	Catalyst		
		3	4	1
2-Hexene	*cis*	30.8	30.8	30.8
2-Hexene	*trans*	50.0	50.0	50.0
3-Hexene	*cis* + *trans*	17.2	11.4	16.4
Coke		2.0	7.8	2.8

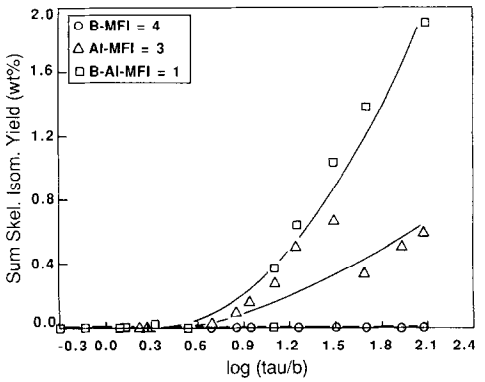

FIG. 7. Skeletal isomer yield as a function of contact time for catalysts 1 = B–Al–MFI; 3 = Al–MFI; 4 = B–MFI.

num centers, both active in the double bond isomerization reaction. The lower activity of boron sites relative to aluminum sites is clearly illustrated by comparison of the activities of catalysts 4 and 3 (Fig. 4d).

Some paraffins are also found in the products. Coke can supply the hydrogen necessary to produce saturated products from olefins. It is difficult to envision how electroneutrality is maintained in that case. We note, however, that paraffins appear only as secondary products and only on catalysts 1 and 3. We therefore propose that they represent fragments of "precoke" oligomers which crack off in the process of coke hardening. The boron catalyst is apparently not able to crack the precoke, resulting in no paraffin production and a greater accumulation of coke on the catalyst.

CONCLUSIONS

A series of catalysts having a contrast aluminum content and increasing amounts of boron was prepared. Boron incorporation in the framework was confirmed both by unit cell volume contraction and by correlation of the integrated absorbance ratio of the 920/550 cm^{-1} bands with boron content.

Our studies of 1-hexene isomerization on all Al-containing catalysts are in line with previous works so that the same reaction mechanism can be assumed. The effect of boron can then be understood using Fig. 6. The parent carbenium ion (I) can rearrange via an H shift to (II), then via a methyl shift to (III) or via the cyclopropyl carbenium ion (IV). From any of these oligomers (V) can also be formed. Both boron and aluminum seem to be effective in the formation of carbenium ion I or II, but only Al appears to be active in skeletal isomerization reactions requiring carbenium ion III or IV as the intermediate. The fact that coke is formed more readily on the boron catalyst suggests that the oligomers formed on this catalyst do not crack and desorb readily. This, too, fits with our understanding that cracking requires strong sites and that large molecules are less likely to desorb.

ACKNOWLEDGMENTS

Thanks are due to Professor J. Abbot (Queen's University, Kingston, Canada) and Dr. L. Basini (Snamprogetti, Italy) for helpful discussions and to Dr. R. Millini (Eniricerche, Milano, Italy) for XRD, SEM, and the chemical analysis work.

REFERENCES

1. Klotz, M. R., Belgian Patent 859658 (1978).
2. Taramasso, M., and Perego, G., *in* "Proceedings, 5th Conf. Zeolites, Naples, 1980," p. 40.
3. Gabelica, Z., and Nagy, J. B., *Chem. Lett.*, 1059 (1984).
4. Coudurier, G., and Vedrine, J. C., *in* "Proceedings, 7th Int. Zeolites Conf., Tokyo, 1987," p. 643.
5. Chu, C. T., and Kuel, G. H., *J. Catal.* **93,** 451 (1985).
6. Hoelderich, W., *in* "Proceedings, 6th Int. Zeolites Conf., Reno, 1984," p. 545.
7. Scholle, K. F. M. G. J., and Kentgens, A. P. M., *J. Phys. Chem.* **88,** 5 (1984).
8. Chang, C. D., and Chu, C. T. W., "American Chemical Society Symp., Miami Beach, 1985," p. 185.
9. Taramasso, M., Italian Patent Application PA22638/A79.
10. Best, D., and Wojciechowski, B. W., *J. Catal.* **47,** 11 (1987).
11. Wojciechowski, B. W., *Catal. Rev. Sci. Eng.* **9,** 79 (1974).
12. Abbot, J., and Wojciechowski, B. W., *J. Catal.* **104,** 80 (1987).
13. Derquane, G., *Appl. Catal.* **1,** 201 (1981).

14. Coudurier, G., and Naccache, C., *J. Chem. Soc. Chem. Commun.*, 1413 (1982).
15. Coudurier, G., and Auroux, A., *J. Catal.* **108,** 1 (1987).
16. Scholle, K. F. M. G. J., and Weeman, W. S., *Zeolites* **5,** 118 (1985).
17. Flanigen, E. M., and Khatami, E. M., *Adv. Chem. Ser.* **101,** 201 (1971).
18. Miecznikowski, A., and Huanuza, J., *Zeolites* **7,** 249 (1987).
19. Tenney, P. G., and Wong, J., *J. Chem. Phys.* **56,** 5516 (1972).
20. Taft, E. A., *J. Electrochem. Soc.* **118,** 1985 (1971).
21. Hornig, D. F., and Plumb, R. C., *J. Chem. Phys.* **26,** 637 (1957).
22. Ko, A. N., and Wojciechowski, B. W., *Int. J. Chem. Kinet.* **15,** 1249 (1983).
23. Abbot, J., and Corma, A., *J. Catal.* **92,** 398 (1985).
24. Maurel, R., and Guisnet, M., *Bull. Soc. Chim. Fr.*, 1975 (1979).
25. National Bureau of Standards, Research Paper 36, p. 559, 1946.
26. Osaka, A., and Takahashi, K., *J. Mater. Sci. Lett.* **3,** 36 (1984).
27. Ghosh, A. K., and Kydd, R. A., *J. Catal.* **100,** 185 (1986).